Arabian Journal of Geosciences (2018) 11: 82
https://doi.org/10.1007/s12517-018-3418-5

ORIGINAL PAPER

Mineralogy, geochemistry, and genesis of the volcanic-hosted hydrothermal iron ore deposit in Somea, NW Iran

Vartan Simmonds[1] · Ali Asghar Calagari[2] · Zahra Sadeghi[2]

Received: 16 September 2017 / Accepted: 30 January 2018 / Published online: 23 February 2018

Abstract
The Somea iron deposit is located ~ 22 km northwest of Ahar, NW Iran. The lenticular iron ores are formed as open space fillings within the pinch and swell structures of a curved fault in a highly brecciated zone within the host andesitic to dacitic rocks. Fe mineralization comprises magnetite and pyrite in the hypogene zone and hematite, limonite, and goethite in the supergene zone. According to the geochemical analysis results, the average grade of Fe ore is about 53 wt%. Magnetite ore is massive and lenticular in shape. Pyrite is formed as veins/veinlets in the crushed zones and fractures within the magnetite ore, following the continued tectonic movements along the fault. Goethite displays spongy and box-work, as well as botryoidal and colloform textures. Spongy and box-work textures indicate the very high acidity of the leaching fluids, which may be resulted from the oxidation of pyrite veins/veinlets. Banded and colloform textures are produced by colloidal precipitation from fluids. Hematite has formed either due to the alteration of magnetite or by dehydration of goethite at the oxidized zone. The very high Fe/Mn ratio of ore samples may indicate the hypogene genesis of the ore-bearing fluids, which were most likely originated from the neighboring Sheyvardagh granitic–granodioritic intrusion. Sulfur isotopic composition of the pyrite samples reveals a magmatic origin for the ore-bearing fluid and its sulfur content, which further advocates the hydrothermal genesis of the ore body. The $\delta^{34}S$ values of the pyrite separates are ranging between − 1.4 and − 0.69‰ (V-CDT).

Keywords Somea · Ahar · Iron ore · Hydrothermal · Sulfur isotope

Introduction

The Somea iron deposit is located at the geographic coordinates of 47° N and 38° 36′ 30″ E, 22 km northwest of Ahar, northwest Iran (Fig. 1). This area forms the southeastern section of the 1:100,000 geologic map of Varzeghan. Based on the structural-geologic classifications of Iran, the Somea area is situated in the Alborz–Azarbaidjan structural zone (Nabavy 1976), Central Iranian Domain (Alavi 1991; Agha Nabaty 2004), on the Tertiary Urumieh–Dokhtar Magmatic Arc (UDMA). The latter is formed through the northeastward subduction of the Neo-Tethyan oceanic crust beneath the Central Iran during the upper Mesozoic-lower Cenozoic (Alavi 1991). This magmatic belt extends from northwest to southeast of Iran over 2000 km (Ghorbani and Bezenjani 2011) with 50-km width (Jahangiri 2007) and more than 4-km thickness (Alavi 1994). The peak of magmatic activity along this belt was during the Eocene (Berberian and Berberian 1981; Alavi 2004).

Preliminary investigations in the studied area showed that the iron ore has been formed as replacements and mostly open space fillings along a fault zone cutting the altered volcanic rocks of Eocene age. The identified ore minerals within hand specimens are mainly Fe oxides, hydroxides, and sulfide. No comprehensive studies have been conducted on different geologic aspects of the Somea iron ore so far. However, in other parts of Iran, especially in northeast of Iran, some detailed studies have been carried out on similar deposits (e.g., Zarabi Rad 2008; Javidi Moghadam et al. 2010; Rajabzadeh and Rasti 2011; Najafzadeh Tehrani et al. 2013).

✉ Vartan Simmonds
simmonds_vartan@tabrizu.ac.ir

[1] Research Institute for Fundamental Sciences, University of Tabriz, 29 Bahman Boulevard, Tabriz 51666, Iran

[2] Earth Sciences Department, University of Tabriz, Tabriz, Iran

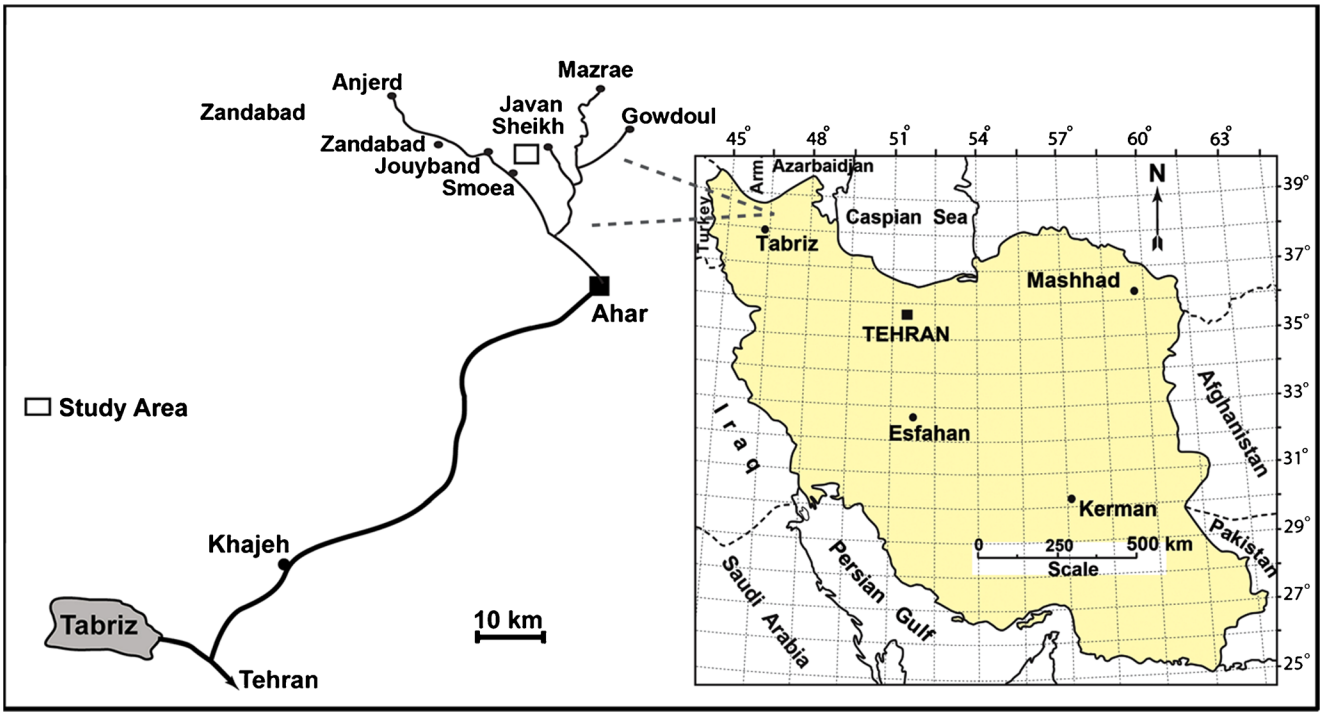

Fig. 1 The location of the study area at northwest Iran and the neighboring Cu-Fe skarn deposits

In the present study, we endeavored to put an emphasis on the economic geology, mineralogy, petrography, Fe transportation and precipitation mechanisms, different stages of alteration and mineralization, and finally the physico-chemical conditions of the ore-bearing fluids. In order to provide a better conception about the mineralization processes in Somea, we considered the geological setting, geometry of the ore body, types and quantity of constituent ore minerals, and mineralogical-geochemical aspects of the studied area. The genesis of the ore was further investigated, and the presented discussions were verified by sulfur isotope analysis on pyrite separates from the hypogene ore.

Geology of the Somea area

The study area shows little lithologic variations, inasmuch as the main part of the Somea area and its environs are covered by acid to intermediate volcanic rocks (Fig. 2; after Mehrpartou et al. (1992) and Mehrpartou and Nazeri (1999)).

The oldest rock units in the vicinity of the study area are the thin-layered limestones (K^{l}) and volcanic-pyroclastic rocks (K^{a}) of upper Cretaceous. Emplacement of the Tertiary Sheyvardagh granitoid body within the K^{l} unit led to the formation of skarn-type Cu and Fe mineralizations around this intrusion at the neighborhood of the Somea iron deposit, which include the well-known Mazrae, as well as Gowdoul, Javan Sheikh, Jouyband, Zandabad and Anjerd Cu–Fe skarns (e.g., Mollaei et al. 2009; Mollai et al. 2009) (Fig. 1).

The most widespread volcanic unit, which is mainly outcropped at the north, east, and south of the Somea village, includes upper Eocene porphyritic dacites to andesites with intercalations of pyroclastic rocks (E^{da}), which have been formed in a submarine environment. These rocks host the iron mineralization. E^{da} unit is laterally terminated by a thick unit of dacitic ignimbrite (E^{ig}). Moreover, trachytic and trachy-andesitic lava flows of the upper Eocene (E^{tc}) cover vast areas at the north and west of the area. Other volcanic rocks of the upper Eocene include mega-porphyritic latite-andesite (E^{lp}) and pyroxene andesite (E^{pa}). In general, these lithologies are laterally equivalent to the E^{da} unit.

Submarine volcanic activities in the Ahar-Varzeghan region almost calmed down at the end of the Eocene and the beginning of Oligocene, when the Eocene marine environment was converted to a sedimentary continental and semi-continental basin. Thereafter, magmatic activities became intrusive in nature, especially in the Oligocene, manifested by small, medium to large intrusive bodies and related andesitic dikes (Ghorbani 2013).

Oligocene and Miocene rock units are not present or outcropping in the study area, and the upper Eocene volcanics are overlain by a trachy-andesite volcanic dome of Pliocene age (Pl^{ta}) at the east of the Somea. However, the

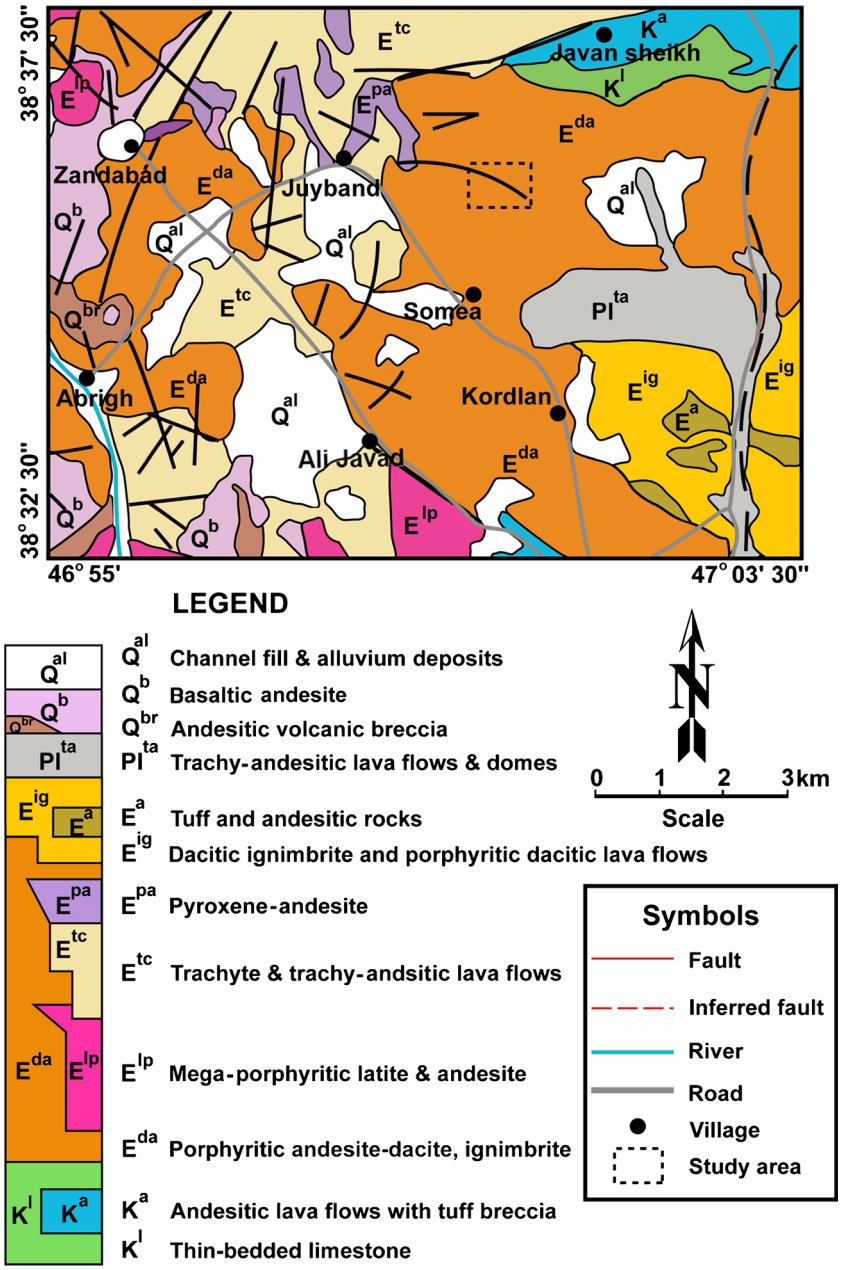

Fig. 2 Geologic map of the Somea area and its environs, modified after the 1:100,000 geologic maps of Kaleybar (Mehrpartou and Nazeri 1999) and Varzeghan (Mehrpartou et al. 1992)

main outcrop of the Oligo-Miocene Sheyvardagh intrusive body is located ~7 km north and northeast of it. Mineralization in the area is attributed to the fluids derived from this intrusion.

Finally, the youngest volcanic rocks in the area are andesite and basaltic andesite rocks of the Quaternary age (Q^b and Q^{br}).

Structurally, many faults are present in this area, mainly striking NW–SE and NE–SW. Considering their strike, it can be conceived that they are contemporaneous with the late Alpine orogenic phases. Post-Eocene continuity of tectonic movements has led to the intersection and displacement of older faults (Mehrpartou et al. 1992).

Materials and methods

Field investigation and geologic study were conducted aiming to identify the rock types, alterations, mineralized zones, and the relationship between tectonic structure and mineralization, as well as to perform systematic sampling of the host rock and the ore body.

Due to the mining activities within the ore body, different parts of the altered host rock and the ore body were easily accessible. Therefore, a systematic sampling was carried out along a 28-m oblique top to bottom profile with a sample per each 2–5-m distance, starting from the almost fresh host rock in the upper part, crossing through the

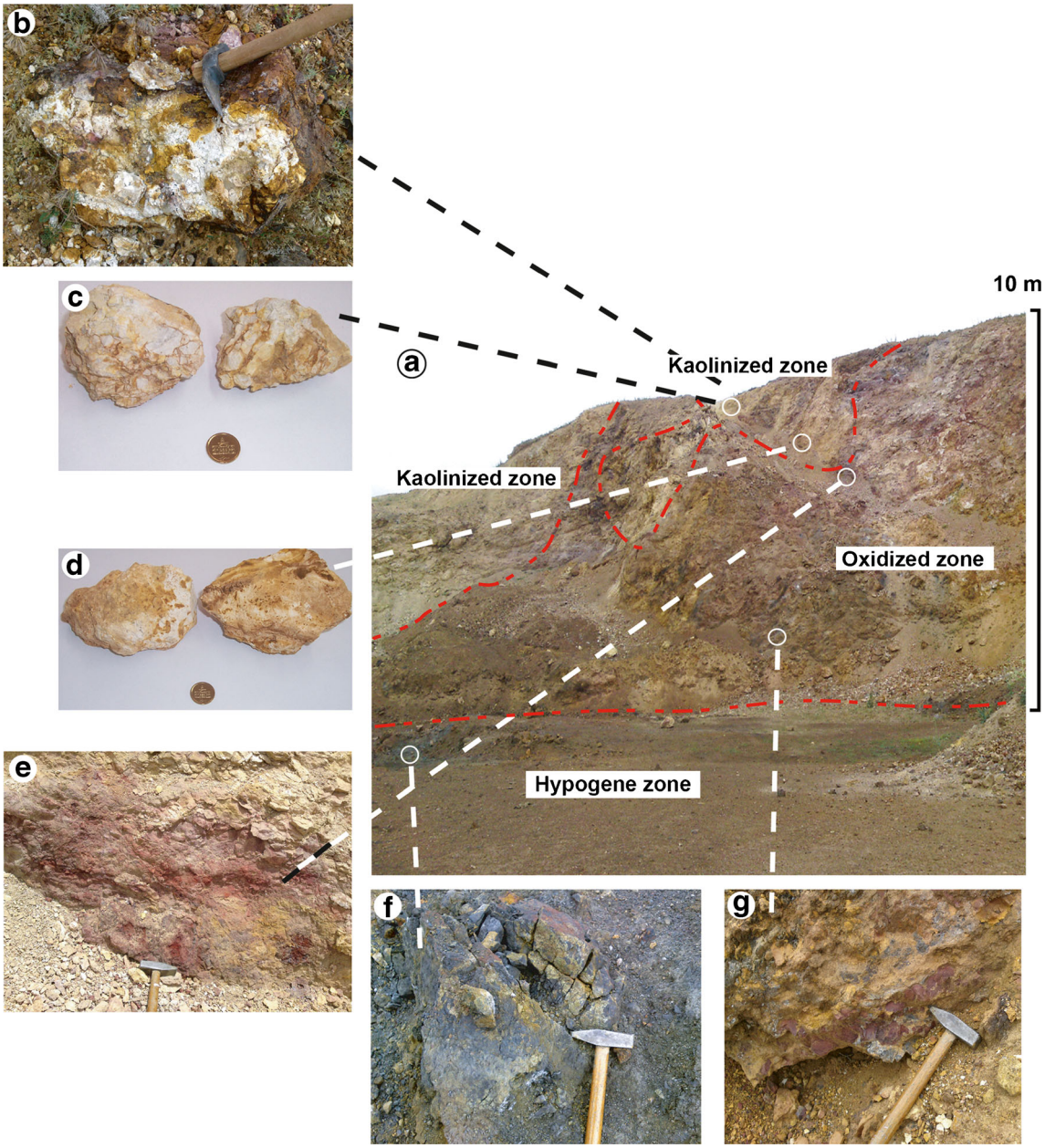

Fig. 3 **a** A sidewall resulted from mining of the iron ore, providing a good outcrop of the kaolinized zone at the upper part of the andesitic to dacitic host rock, the supergene oxidized ore at the middle part, and the hypogene zone at the lower part. **b**, **c, d** Hand specimens of keolinized Fe-bearing host rock. **e** The supergene oxidized zone comprised of hematite and goethite. **f** Hypogene ore including massive magnetite with pyrite veins and veinlets. **g** Supergene oxidized zone with brecciated texture

supergene oxidized ore and patches of altered host rock and finally reaching to the hypogene ore zone in the lowermost part of the section (Fig. 3). The location and physical characteristics of each sample are shown in Table 1. Additionally, a horizontal sampling was also done from the host rock towards the center of the ore body.

Besides the petrographic and mineralographic studies on the polished thin sections prepared from collected samples, 10 systematically collected samples along the selected profile were analyzed for major, minor, trace, and rare earth elements in the LabWest laboratory (Australia), using inductively coupled plasma optical emission spectrometry (ICP-OES) and inductively coupled plasma mass spectrometry (ICP-MS) methods for major and trace elements, respectively (Table 2).

In addition, six samples from this profile were analyzed by X-ray diffraction (XRD) method in order to identify mineral phases within the highly altered host rock and the oxidized supergene and hypogene ores, using Siemens D500 X-ray powder diffractometer with Ni-filtered Cu-

Table 1 Physical characteristics and the location of samples collected along the oblique profile

Sample no.	Physical characteristics	Distance (m)
S1	Almost fresh host rock with weak alteration	0
S2	Supergene ore with relatively high amount of kaolinized host rock fragments	5
S3	Supergene oxide ore	10
S4	Supergene ore containing ochre hematite with kaolinized host rock fragments	12
S5	Supergene ore with kaolinized host rock fragments	16
S6	Supergene oxide ore	20
S7	Supergene oxide ore with spongy and box-work textures	22
S8	Micaceous hematite ore at the margin	23
S9	Hypogene magnetite-pyrite ore	25
S10	Hypogene magnetite-pyrite ore	28

Kα source and graphite diffracted beam monochromator at the X-ray laboratory of the Faculty of Physics, University of Tabriz.

Four pyrite separates collected from hypogene ore were analyzed for sulfur isotope composition in UC Davis stable isotope facility, University of California, USA. Stable isotope ratios of ^{34}S were measured using an Elementar vario ISOTOPE cube interfaced to a SerCon 20-22 IRMS (Sercon Ltd., Cheshire, UK). Samples were combusted at 1150 °C in a reactor packed with tungsten oxide. Immediately following combustion, sample gases were reduced with elemental copper at 880 °C and subsequently passed through a buffering reactor filled with quartz chips held at 900 °C. SO_2 and CO_2 were then separated by purge and trap, allowing for full separation and peak focusing. Following separation, the SO_2 adsorption trap was heated and the sample SO_2 passed directly to the IRMS for measurement.

During isotopic analysis, samples were interspersed with replicates of several laboratory reference materials to monitor and allow for correction of any potential variation in drift and linearity. Final $\delta^{34}S$ values were obtained after adjusting the provisional measurements such that correct $\delta^{34}S$ values for laboratory quality assurance materials were obtained. Laboratory reference materials were calibrated directly against IAEA S-1, S-2, and S-3, as well as NBS-127, SO-5, and SO-6. The long-term reproducibility of this method is ± 0.4‰.

Results

Petrography of the host volcanic rocks

Based on the 1:100,000 geologic maps of Varzeghan and Kaleybar, as well as the petrographic studies, volcanic host rocks of the Somea Fe ore were classified as andesites to dacites. The main rock-forming mineral is plagioclase (50–60%, 1–4 mm), occurring as euhedral to subhedral phenocrysts with Carlsbad and polysynthetic twining, as well as microlites within the groundmass (Fig. 4a, b). Relicts of ferro-magnesian minerals are scattered within the groundmass (10–20%, < 1 mm). Biotite (0–5%) is completely altered and is recognizable by its book shape and replacement by muscovite. Amphiboles (5–15%) are also recognizable by their shape, crystallographic planes, and their alteration to sericite and tremolite (Fig. 4c, d). Fine anhedral grains of quartz (5–10%) and opaque minerals (mainly Fe oxides, 5–10%, occurring as disseminated fine subhedral to anhedral crystals within the groundmass, as well as veinlets and micro-veinlets) are other constituents of these rocks (Fig. 4). The volcanic host rocks display porphyritic texture with fine-grained to microlitic groundmass.

All these rocks experienced later-stage sericitic and argillic alterations, which are intensified towards the ore body (Fig. 4), testifying to their formation by hypogene fluids. XRD analysis results show the presence of kaolinite, montmorillonite, and jarosite in this zone.

Description of the Somea ore deposit and the paragenetic sequence

Fe mineralization in Somea is in the form of elongated lenses. These lenses occur successively along a curved fault with NW–SE general trend (Fig. 2) and mainly sharp contact with the host rock. Besides filling the spaces within the fault breccia, the ore material is also brecciated itself (Fig. 3f), which may confirm the activity of the fault after the mineralization. Therefore, field investigations indicate that these lenses are formed as replacements and open space fillings within the pinch and swell structures along the fault in the host andesitic to dacitic (E^{da}) rocks. The main lenticular ore body, which is mined at the moment, has an approximate trend of ENE–WSW, ~ 200-m length and 70-m width. According to the geochemical analysis data of the ore samples, the Fe grade ranges from 35.6 to 68.5 wt% (with an average of ~ 53 wt%) (Table 2).

Table 2 Analysis results of the andesitic host rock and supergene and hypogene ore samples of the Somea iron ore. Sample descriptions are as Table 1

Element	D.L. (ppm)	S1	S2	S3	S4	S5	S6	S7	S8	S9	S10
Al	10	10.1%	1650	1980	2780	9780	4110	1850	1700	8540	2.63%
Na	10	1820	1.19%	76	167	1250	1670	585	57	150	178
K	10	4.38%	2.38%	156	377	3140	2290	2840	252	1460	1660
Ca	10	4540	350	279	541	3830	526	289	304	3750	1410
Mg	10	1160	292	165	72	2810	374	44	1200	1.71%	3050
Fe	100	6.37%	35.6%	53.7%	45.6%	51.0%	57.4%	53.8%	68.5%	59.4%	51.8%
Ti	10	4970	1590	895	2110	2440	917	3520	171	862	660
Mn	2	53	2810	814	233	670	1500	81	4370	2960	1980
P	5	2010	569	344	711	2300	2150	2530	< 5	571	866
S	50	53	6.03%	5520	6910	9110	1.03%	1.18%	1470	2.58%	16.8%
Ag	0.01	0.20	6.1	0.85	1.9	0.65	1.6	1.1	0.23	0.33	1.5
As	0.5	21.5	362	184	463	194	162	3890	326	118	312
Ba	0.2	386	607	47.8	163	275	1580	269	128	106	368
Be	0.2	2.0	< 0.2	0.4	0.2	0.4	2.7	0.4	1.1	2.7	1.9
Bi	0.1	1.8	7.2	3.7	14.6	2.0	3.5	45.8	0.5	1.9	6.7
Cd	0.05	0.15	0.07	0.07	0.11	0.28	0.45	0.22	0.17	3.91	0.61
Co	0.2	1.3	4.8	2.1	1.0	5.3	5.1	1.6	2.6	29.4	80.2
Cr	2	5	46	12	23	91	37	9	< 2	8	14
Cs	0.1	5.4	1.0	0.1	0.5	0.7	0.3	0.1	0.1	1.1	1.1
Cu	0.2	24.0	63.2	197.8	263.6	117.9	185.2	81.7	6.8	4.0	239.4
Ga	0.05	23.9	11.3	5.18	6.79	32.2	11.1	5.56	3.96	6.86	24.6
Ge	0.05	2.27	2.64	1.95	2.27	3.43	1.40	2.00	1.20	2.0	2.29
Hf	0.02	0.86	0.39	0.12	0.29	0.90	0.09	0.65	0.09	0.11	0.10
Hg	0.05	< 0.05	< 0.05	< 0.05	< 0.05	< 0.05	< 0.05	< 0.05	< 0.05	< 0.05	< 0.05
In	0.01	0.28	1.05	0.52	0.52	0.80	0.63	0.27	0.53	1.03	1.51
Li	0.5	7.99	2.5	< 0.5	< 0.5	14.6	< 0.5	2.9	5.5	1.38	336
Mo	0.1	6.0	7.4	6.1	4.2	39.5	8.4	49.8	1.1	0.8	1.8
Nb	0.5	3.1	7.2	4.4	7.4	10.9	3.8	8.8	2.9	3.3	5.6
Ni	2	4	2	5	3	6	5	4	9	18	75
Pb	0.2	2.45	112	24.2	28.6	63.8	347	189	42.3	0.50	19.3
Rb	0.1	185	41.6	0.4	1.8	15.4	11.4	3.3	1.0	4.6	4.6
Re	0.01	< 0.01	< 0.01	< 0.01	< 0.01	< 0.01	< 0.01	0.01	< 0.01	< 0.01	< 0.01
Sb	0.1	4.4	13.4	6.3	6.9	9.9	5.6	140	10.7	6.7	7.1
Sc	1	13	< 1	< 1	1	2	< 1	< 1	< 1	1	6
Se	0.05	0.98	20.4	6.34	26.7	10.9	0.86	14.7	0.23	0.53	1.19
Sn	0.2	3.9	11.3	12.7	20.4	2.9	11.4	28.8	35.6	12.8	18.6
Sr	0.1	618	454	17.3	17.4	242	293	30.2	8.7	19.4	193
Ta	0.01	< 0.01	0.42	0.20	0.20	0.43	0.04	0.60	0.84	0.06	0.11
Te	0.2	2.7	2.7	3.6	12.2	2.0	3.7	26.2	2.0	0.4	1.6
Th	0.02	1.01	1.62	1.44	2.78	3.96	2.61	2.34	0.61	0.82	1.71
Tl	0.1	2.4	13	< 0.1	< 0.1	0.8	0.6	2.1	0.2	0.3	0.2
U	0.02	1.77	1.17	0.56	0.94	2.82	2.48	1.11	0.29	1.16	2.86
V	2	197	53	63	111	520	55	44	22	29	26
W	0.1	1.9	2.2	2.1	2.2	0.6	1.6	4.3	1.1	4.8	2.9
Y	0.05	8.43	9.87	2.40	10.6	6.39	3.27	1.7	2.33	10.2	9.82
Zn	0.2	70.9	12.6	83.0	48.8	174	387	343	230	856	501
Zr	1	18	16	5	10	34	2	19	3	2	3
La	0.05	7.99	2.21	2.55	5.45	25.2	12.6	2.13	0.72	1.38	336

Table 2 (continued)

Element	D.L. (ppm)	S1	S2	S3	S4	S5	S6	S7	S8	S9	S10
Ce	0.05	14.7	2.23	4.17	10.2	33.4	15.0	2.64	1.77	2.95	317
Pr	0.05	2.45	0.27	0.54	1.58	3.99	1.46	0.30	0.27	0.50	19.3
Nd	0.02	10.5	1.24	2.15	7.67	13.4	4.55	1.06	1.30	2.51	45.6
Sm	0.02	2.54	0.56	0.48	1.87	1.96	0.86	0.21	0.38	0.85	5.67
Eu	0.02	0.75	0.28	0.12	0.54	0.50	0.37	0.06	0.07	0.29	0.92
Gd	0.05	1.91	0.99	0.43	1.33	2.45	1.99	0.31	0.34	0.79	26.8
Tb	0.02	0.30	0.17	0.06	0.25	0.15	0.10	0.03	0.08	0.23	0.78
Dy	0.02	1.95	1.01	0.35	1.42	0.79	0.53	0.22	0.41	1.31	3.03
Ho	0.02	0.27	0.24	0.08	0.28	0.15	0.10	0.05	0.09	0.28	0.42
Er	0.05	0.78	0.72	0.22	0.83	0.42	0.30	0.22	0.25	0.77	1.10
Tm	0.05	0.13	0.12	< 0.05	0.13	0.17	< 0.05	0.05	< 0.05	0.11	0.14
Yb	0.05	1.73	0.79	0.21	0.69	0.47	0.44	0.40	0.20	0.61	0.83
Lu	0.02	0.15	0.08	0.03	0.08	0.05	0.03	0.08	0.4	0.10	0.13

Based on field observations, microscopic studies, and mineral assemblages, two stages can be tracked for the evolution of the ore bodies in the study area. The primary or hypogene ore is characterized by magnetite and pyrite (Fig. 5a), which is found at deeper levels and beneath the supergene oxidized zone.

By taking into account the mineralographic and XRD results, magnetite (50–80%) is the most abundant and the main hypogene mineral in Somea. It is massive and dense with brecciated and occasionally granular texture (Fig. 5a–c). Martitization is evident in most samples taken from upper parts of the hypogene ore, while in deeper levels, magnetite is almost fresh. XRD analysis data also reveal the presence of maghemite along with magnetite in the hypogene ore.

Pyrite (5–50%) occurs as 1 mm to > 10-cm-thick veins/veinlets (Fig. 5a, d, e) within the predominantly magnetite ore. These veins and veinlets show cross-cutting and brecciated texture and contain fine to medium-grained (< 100 μ m up to 3–4 mm) euhedral to subhedral pyrite crystals (Fig. 5d, e). The rate and the intensity of later-stage brecciation are higher within the pyrite veins/veinlets compared to the magnetite ore, as their reopening would be much easier compared to the other parts, and therefore, even the occurrence of last-stage calcite and silica (< 100 μm to 2 mm thick) micro-veinlets within the pyrite

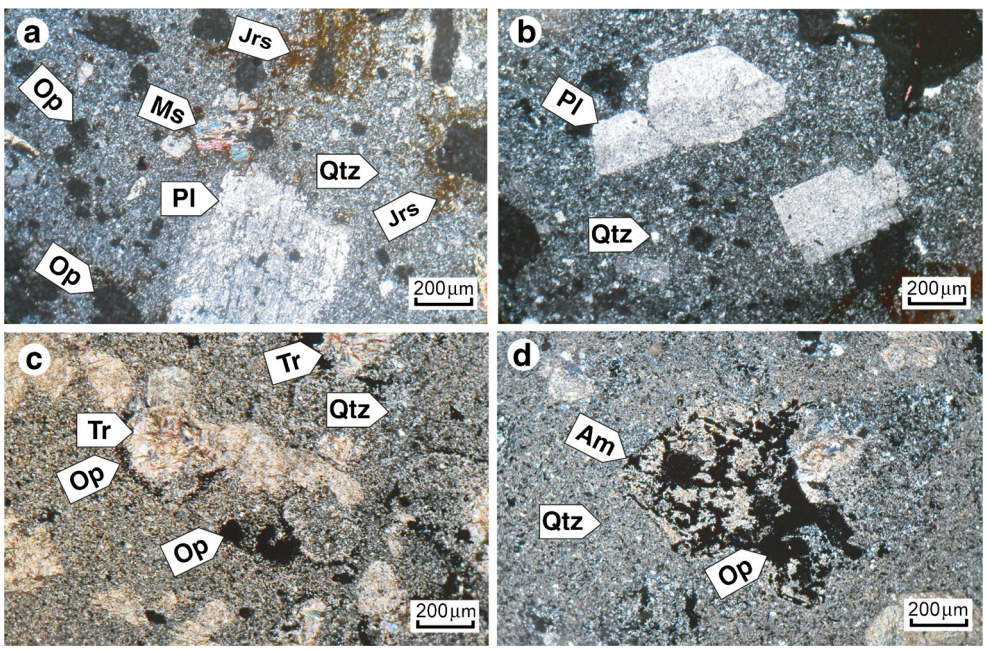

Fig. 4 Photomicrographs of E^{da} volcanic rocks. **a** Plagioclase phenocrysts are highly kaolinized, and biotites are replaced by muscovite and opaque minerals in a microcrystaline groundmass. Traces of jarosite are also visible. **b** Euhedral altered plagioclase phenocrysts with Carlsbad twining. **c** Replacement of ferro-magnesian minerals by tremolite, sericite, and Fe oxides, alteration of plagioclases to sericite. **d** Pseudomorph of a euhedral amphibole phenocryst, replaced by sericite and released lots of Fe oxide. Mineral abbreviations from Whitney and Evans (2010)

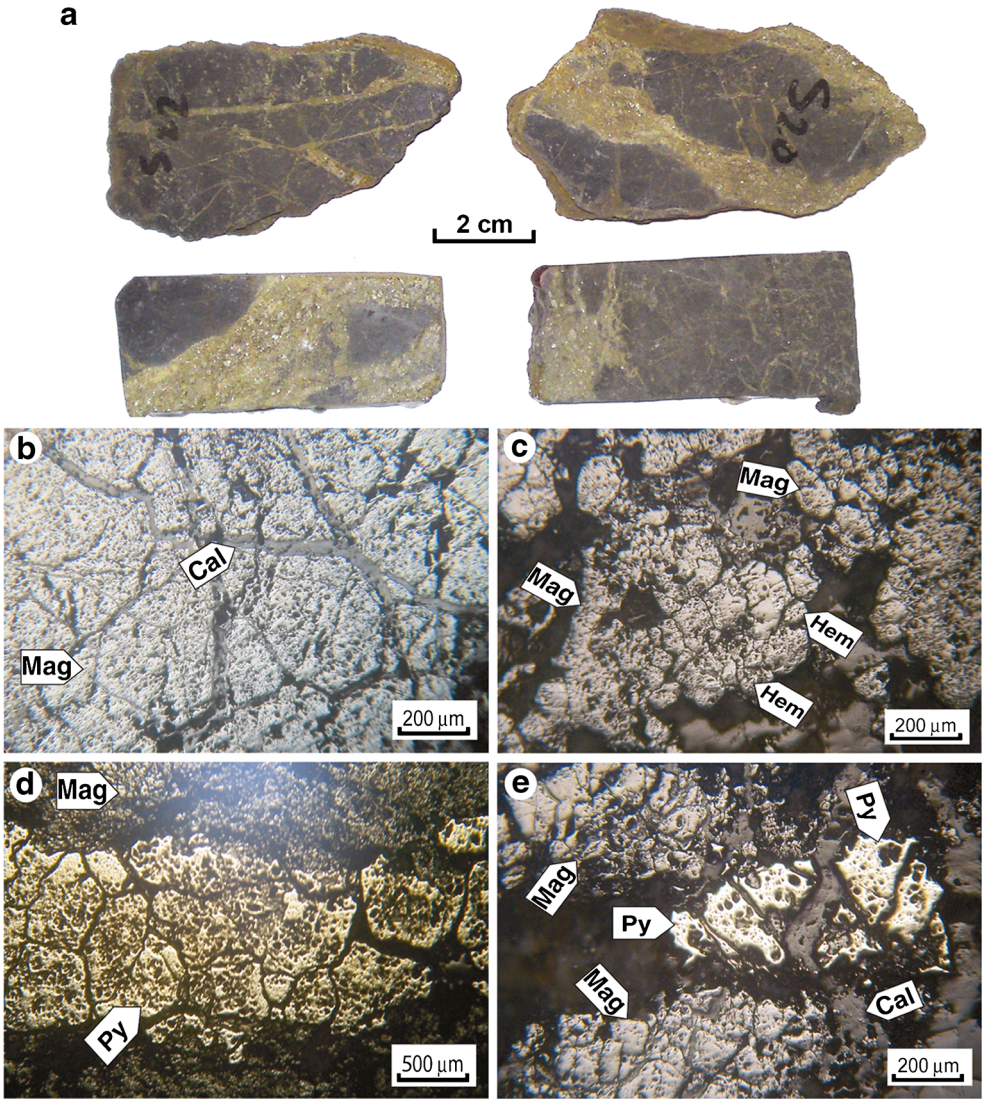

Fig. 5 Mezoscopic and microscopic photos of hypogene ore minerals. **a** Vein-type occurrence of pyrite within the magnetite ore. **b** Calcite micro-veinlets within the massive and brecciated magnetite ore. **c** Anhedral granular martitized magnetite. **d** A brecciated pyrite vein within the magnetite ore. **e** Anhedral pyrite grains filling the open spaces and fractures within the magnetite ore, both of which were subsequently cross-cut by calcite veinlets and micro-veinlets. Mineral abbreviations from Whitney and Evans (2010)

veins and veinlets is much more relative to the magnetite ore (Fig. 5b, e).

The hypogene ore was later subjected to supergene alteration and intense oxidation, characterized by the replacement of pyrites by Fe oxides and hydroxides, including hematite, goethite, limonite, and jarosite and the conversion of magnetite to hematite (martitization) and goethite. The thickness of the oxidized supergene zone is ~ 10 m (Fig. 3a).

Goethite is abundantly found in the oxidized ore of the Somea area. It has spongy and box-work, as well as botryoidal and colloform textures (Fig. 6a–d) and is accompanied by lesser limonite and hematite (Fig. 6c, d).

One piece of evidence implying the pre-existence of pyrite at the supergene zone of the ore body is the formation of jarosite [$KFe_3^{(+3)}(SO_4)_2(OH)_6$] and natrojarosite [$NaFe_3^{(+3)}(SO_4)_2(OH)_6$] with brownish yellow color, which is distinguished by the field observations, petrographic studies (Fig. 4a), and XRD analysis.

According to mineralographic studies, hematite has been formed by alteration of magnetite and dehydration of goethite (Figs. 5c and 6c, g, h). In general, the hematite content of the supergene ore reaches up to 80% in some samples.

Sulfur isotope data

In order to study the isotopic composition of sulfur in pyrites within the hypogene ore, four mineral separates were analyzed, results of which are presented in Table 3. Sulfur content of the analyzed pyrite separates range from 201 to 221.1 μg (mean = 211.2 μg). The measured $\delta^{34}S$ values of pyrite range from − 1.40 to − 0.69‰ Vienna Cañon Diablo troilite (V-CDT), with an average of − 0.91‰ V-CDT, revealing near-zero values. Three internal standard materials with known $\delta^{34}S$ were analyzed 5 to 10 times during the analysis of Somea samples in order to check the reproducibility and precision of the measurements. The obtained results showed that

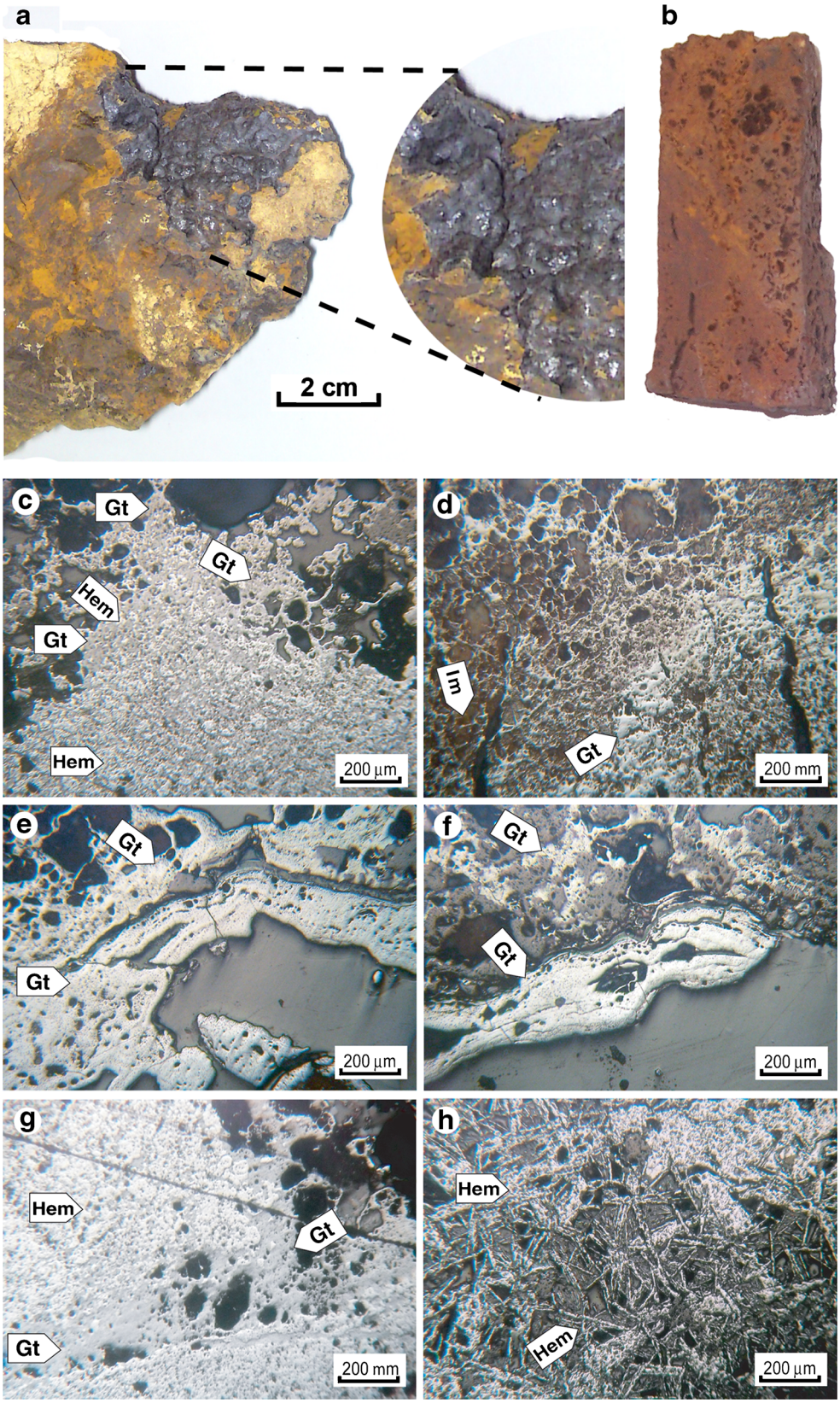

Fig. 6 Mezoscopic and microscopic photos of samples from the supergene oxidized ore. **a** Botryoidal and colloform texture of goethite. **b** Spongy and honeycomb textures of supergene oxidized ore (mainly goethite). **c**, **d** Alteration of hypogene ore to goethite, hematite, and limonite with spongy texture. **e**, **f** Banded texture of goethite ore. **g** Hematite ore with the evidence of hydration and the formation of goethite along a fracture. **h** Micaceous hematite. Mineral abbreviations from Whitney and Evans (2010)

the measured and the mean values of the reference materials are very close to their reported isotopic composition, only showing very low standard deviation, which may testify that the precision of the obtained results is acceptable.

Table 3 Sulfur isotopic composition of four pyrite samples from the hypogene ore in Somea, and the analysis results of the standard materials

Sample		δ^{34}S vs. V-CDT ()	S (μg)
P1		− 1.40	201.0
P2		− 0.88	210.8
P3		− 0.69	211.9
P4		− 0.69	221.1
Measured δ^{34}S on standard 1 (V-CDT)		Measured δ^{34}S on standard 2 (V-CDT)	Measured δ^{34}S on standard 3 (V-CDT)
18.31		2.17	− 3.91
18.50		1.89	− 3.84
18.55		1.85	− 4.14
18.53		1.88	− 4.06
18.67		2.10	− 3.74
18.70			
18.79			
18.78			
18.29			
18.06			
Mean	18.52	1.98	− 3.94
SD	0.24	0.15	0.16
Reported δ^{34}S	18.15	1.91	− 3.94

Discussion

Interpretation of mineralogy and ore texture

As it was described previously, the lenticular, patchy, and open-space filling structure of the Somea iron ore indicates the role of tectonic activities in preparing a favorable space for infiltration of ore-bearing fluids and subsequently precipitation of iron ore minerals. The presence of brecciated fragments of the host rock cemented by the ore minerals further advocates the role of secondary structural permeability. Mineralization within the crushed and faulted zones (including the pre-existence of fault breccia) and the presence of Fe-bearing patches, veins, and veinlets within the host rock with sharp contact, which have subsequently been brecciated during the later tectonic movements, indicate the epigenetic nature of the Somea Fe ore deposit.

Based on field and mineralographic studies, hypogene mineralization has occurred in three stages. Magnetite was the first opaque phase precipitated from the hypogene ore-bearing fluids (first stage). Tectonic movements after the formation of magnetite ore led to the brecciation of pre-existing ore body, and following the compositional changes of ore-bearing fluids, which will be discussed later, the resulted fractures and open spaces formed within the magnetite ore were filled with pyrite as veins/veinlets (second stage). Their cross-cutting and brecciated texture indicates the continuous and repeated tectonic movements and penetration of ore-bearing fluids in the area (Fig. 5d, e).

Finally, following the intermittent tectonic movements and brecciation of the ore body, the resulted micro-fractures and open spaces within the hypogene ore were filled with calcite and quartz, which represent post-mineralization fluids (third stage). These veinlets and micro-veinlets (< 1–2 mm thick) are mainly concentrated within the pyrite veins-veinlets as the weak areas of the ore body.

The hypogene ore above the water table subsequently subjected to supergene alteration, which led to its extensive oxidation. The presence of pyrite veins/veinlets had a considerable impact on escalating the acidity of the descending surface waters, leading to the enhanced dissolution and leaching of the host rock clasts and patches within the mineralized zone and the formation of cavities and boxwork texture. Furthermore, the high permeability of the area due to the presence of numerous fractures and brecciated texture facilitated the penetration and percolation of acid and O_2-rich meteoric waters and hence the oxidation of the hypogene ore.

According to mineralographic studies and XRD results, goethite is the main ore mineral in the oxidized zone, which is the most stable Fe oxide mineral under the oxidizing and supergene conditions. Its spongy and boxwork textures indicate the very high acidity of the leaching fluids, inasmuch as the clasts of the host rock are completely dissolved and only traces of quartz are left behind. Banded and colloform textures are produced by colloidal precipitation from fluids (Fig. 6a, e, f). Colloidal precipitations (gels) are meta-stable and form microcrystalline aggregates of banded, colloform, and botryoidal

textures by losing water. Such textures within the goethites of the Somea deposit indicate the presence of Fe-bearing colloidal fluids at the supergene stage, which slowly precipitated Fe oxides within the open spaces and fractures. Considering the widespread occurrence of sulfide veins/veinlets within the hypogene ore, formation of such solutions at the supergene stage seems to be rational. Finally, the skeletal texture is also common within the supergene ore, testifying to the presence of abundant Fe sulfides in the hypogene ore body prior to the supergene alteration.

Hematite is another constituent of the oxidized zone. Two generations of hematite are distinguished in Somea deposit: (1) those produced by the alteration of magnetite and its martitization, especially at the upper and oxidized parts of the ore body (Figs. 5c and 6c) and (2) those resulted from dehydration of goethites at the oxidized zone (Fig. 6g, h) (Maynard 1983), which are found as micaceous hematite (specularite) with silvery luster. Remnants of goethites are visible as islands within the second generation of hematite.

Jarosite and natrojarosite are formed under low pH condition and by the destruction of Fe-bearing minerals (Bigham et al. 1996). Sulfur required for their formation is provided by the oxidation of pyrite; potassium is derived from the alteration of K-feldspars and biotite in the host rock, while Na is supplied by the alteration of plagioclase.

Genesis of the Somea iron ore based on geochemical and sulfur isotope data

The main criterion to determine the genesis of iron ores is the Fe/Mn ratio. This ratio ranges from > 0.1 to < 10 in hydrothermal deposits (Nicholson 1992), showing the intense differentiation of these elements within the transporting fluids. The Fe/Mn ratio is between 126 and 382 in the analyzed ore samples and indicates a hydrothermal origin. In addition, Fe-Mn-(Co+Ni+Cu)×10 diagram (Fig. 7; Toth 1980) also reveals a hydrothermal origin for the studied ore. On the other hand, hydrothermal fluids are not able to transport high Co and Ni contents (Meinert 1995), which is manifested by the low Co and Ni contents in the Somea ore. The Ni/Co ratio is also used to determine the genesis of iron ores (Bajwah et al. 1987), which ranges between 0.2 and 7 in hydrothermal deposits. This ratio is about 0.42–3.46 in Somea ore, which may testify to its hydrothermal origin. Meanwhile, the Co/Ni range of 1 to 10 is defined as a characteristic feature of the hydrothermal origin (Bajwah et al. 1987); most of the Somea ore samples, especially those of the hypogene zone, fall in this range.

Based on Table 3, the $\delta^{34}S$ values of pyrite are between −1.40 and −0.69‰ V-CDT, with an average of −0.91‰ V-CDT. The near-zero values of all isotopic data may suggest that sulfur within the ore-forming fluids was derived from a magmatic source (Ohmoto and Rye 1979; Faure 1986) and further confirm the hydrothermal genesis of the ore formation.

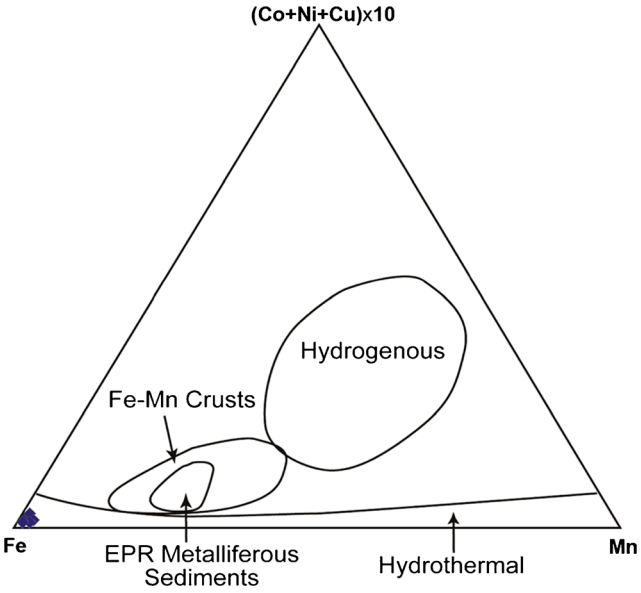

Fig. 7 Fe-Mn-(Co+Ni+Cu)×10 diagram (Toth 1980) to discriminate the genesis of the iron ores

The negative to near-zero $\delta^{34}S$ values of pyrite samples and the lack of primary sulfate minerals accompanying pyrite suggest that the ore-bearing fluids had relatively low pH and fO_2 during the pyrite precipitation stage (Ohmoto 1972; Faure 1986), resulting in the sufficiently low mole fraction of SO_2 gas (at temperatures above 400 °C; Ohmoto and Rye 1979) or SO_4^{2-} (at temperatures below 400 °C) in the ore-bearing fluids, so that H_2S was prevailing during the sulfide precipitation.

Finally, the lack of silicate minerals characteristic of skarn deposits (e.g., garnet, epidote, pyroxene, and actinolite) within the host rocks or accompanying the ore and the lack of intrusive bodies and carbonate rock outcropping in the study area are against any speculations about skarn-type origin for Somea ore.

Physico-chemical characteristics of the ore-bearing fluids

Hypogene mineralization in Somea was emerged by the precipitation of magnetite. Its formation from acid and oxidant ($Fe^{3+} > Fe^{2+}$) magmatic hydrothermal fluids can be explained by the following reaction (Paterson and Cloos 2005):

$$2FeCl_3 + FeCl_2 + 4H_2O = Fe_3O_4 + 8HCl \quad (1)$$

The hydrothermal fluids containing chloride complexes were most likely derived during the differentiation and crystallization of the Sheyvardagh intrusive body and might have experienced mixing with groundwaters of meteoric origin

during their ascend upward. These fluids may also have reacted with the upper Cretaceous carbonate rocks probably underlying the Eocene volcanics, outcrops of which are found at the neighboring Javan Sheikh area, ~4 km NE of it. Changes in physical characteristics of the hydrothermal fluids, including temperature decrease during their mixing with low-temperature surficial fluids or pH increase upon reaction with carbonate rocks, as well as sudden pressure drop and expansion due to infiltration into a brecciated and crushed fault zone caused severe instability of metal–chloride complexes and precipitation of ore materials.

Ulrich and Heinrich (2002) believe that during the early stages of the evolution of magmatic-hydrothermal deposits, fluids responsible for mineralization are undersaturated in respect of sulfide and contain SO_2 as the dominant sulfur species (Clark and Arancibia 1995). This feature along with the high fO_2 has led to the occurrence of oxide mineralization at the first stage of Somea ore formation.

Subsequently, by the consumption of ore-bearing fluid's oxygen content through the magnetite precipitation, fO_2 gradually decreased within the infiltrating fluids and led to the dominance of H_2S species in them. However, Landtwing et al. (2005) argue that by considering the HCl production as the result of reaction (1) during the magnetite precipitation, sulfide cannot reach to saturation limit independent of temperature decrease. On the other hand, hydrolysis of SO_2 to H_2S can occur by the temperature decrease to about 400 °C (Holland and Malinin 1979). Many authors believe that these changes may result in sulfide mineralization (e.g., Burnham and Ohmoto 1980; Hemley and Hunt 1992; Wood 1998; Paterson and Cloos 2005). The reaction proposed for pyrite precipitation is as follows (Paterson and Cloos 2005):

$$3FeCl_2 + 5H_2S + SO_2 = 3FeS_2 + 6HCl + 2H_2O \quad (2)$$

Sulfide mineralization in Somea occurred in this way as veins/veinlets within the massive magnetite ore, filling the fractures and crushed zones resulted from periodic tectonic activity along the fault zone.

According to the stability fields of oxide and sulfide minerals in hydrothermal systems (Einaudi et al. 2003) and considering the paragenesis of the Somea ores, the sulfidation state of the ore-forming fluids was low at the magnetite precipitation stage, which increased to the intermediate level during the pyrite mineralization. According to Log_{aO2}-Log_{aS2} diagram presented by Henley et al. (1984) for oxide and sulfide minerals, Log_{aO2} at the magnetite stage was between − 38.5 and − 34.5, corresponding to Log_{aS2} values of − 14 to − 11. However, during the pyrite precipitation, Log_{aS2} increased up to − 9. Meanwhile, based on the Log_{fO2}–pH diagram proposed by John et al. (1999) for hydrothermal alterations and mineralizations, and considering the formation of sericite and kaolinite within the altered host rocks, the pH range of the ore-bearing fluids was 4–5.5.

At the supergene stage, magnetite (due to having Fe^{2+} in its structure) became unstable upon being subjected to oxidizing conditions and transformed to Fe^{3+} oxides. Sulfides (pyrite in this case) are also unstable under the supergene and oxidizing conditions and give rise to Fe oxides/hydroxides and H_2SO_4. The latter also leads to an increase in the acidity of descending supergene fluids and intensifies the supergene alteration (Bigham and Nordstrom 2000). Meanwhile, the produced $Fe^{3+}[Fe_2(SO_4)_3]$ acts as an important oxidizing agent for Fe sulfides in acid conditions.

Conclusions

The Somea iron deposit was showed to have hydrothermal origin, most likely related to the magmatic-hydrothermal systems affiliated to the neighboring Sheyvardagh granitic–granodioritic intrusion of Oligo-Miocene age. This intrusive body was emplaced in the upper levels of the continental crust within the upper Cretaceous carbonate rocks and produced some skarn-type Cu and Fe mineralizations such as Mazrae and Anjerd around it. This intrusive body was most likely the supplier of heat, fluids, and ore materials for the Somea iron deposit. Hydrothermal fluids have also produced intense sericitic and argillic alteration within the host volcanic rocks. Temperature decrease, pH increase upon probable reaction with carbonate rocks upon migration, as well as sudden pressure drop due to infiltration into the brecciated and crushed fault zone, which enhanced the cooling rate and increased the pH through the loss of volatile acid constituents, are found to be the main factors leading to the precipitation of ore materials. Sulfide mineralization emerged following the consumption of the ore-bearing fluid's oxygen content in the form of magnetite and the dominance of H_2S species within the hydrothermal fluids concomitant with the temperature decrease.

Acknowledgements Authors would like to express their thanks and appreciation to the authorities in the Research Bureau of the University of Tabriz for their financial support. Our appreciation is further expressed to the anonymous reviewers for making critical comments and valuable suggestions on this manuscript.

Funding information This study was financially supported by the Deputy Dean of the Research Bureau of Tabriz University through the grant no. 90213.

References

Agha Nabaty E (2004) Geology of Iran. Geological survey and mineral exploration organization of Iran, Tehran, p 586 (in Persian)

Alavi M (1991) Sedimentary and structural characteristics of the paleo-Tethys remnants in northeastern Iran. Geol Soc Am Bull 103(8):

983–992. https://doi.org/10.1130/0016-7606(1991)103<0983:SASCOT>2.3.CO;2

Alavi M (1994) Tectonics of the Zagros orogenic belt of Iran: new data and interpretations. Tectonophysics 229(3-4):211–238. https://doi.org/10.1016/0040-1951(94)90030-2

Alavi M (2004) Regional stratigraphy of the Zagros fold-thrust belt of Iran and its proforeland evolution. Am J Sci 304(1):1–20. https://doi.org/10.2475/ajs.304.1.1

Bajwah ZU, Secombe PK, Offler R (1987) Trace element distribution, Co:Ni ratios and genesis of the big Cadia iron–copper deposit, New South Wales, Australia. Mineral Depos 22:292–300

Berberian F, Berberian M (1981) Tectono-plutonic episodes in Iran. In: Gupta HK, Delany FM (eds) Zagros, Hindu Kush, Himalaya: geodynamic evolution. Geodyn ser, Am Geophys Union 3:5–32. https://doi.org/10.1029/GD003p0005

Bigham JM, Nordstrom DK (2000) Iron and aluminum hydroxyl-sulfates from acid sulfate waters. In: Alpers CN, Jambor JL, Nordstrom DK (eds) Sulfate minerals: crystallography, geochemistry and environmental significance. Rev Mineral Geochem 40:351–403. https://doi.org/10.2138/rmg.2000.40.7

Bigham JM, Schwertmann U, Traina SJ, Winland RL, Wolf M (1996) Schwertmannite and the chemical modeling of iron in acid sulfate waters. Geochim Cosmochim Acta 60(12):2111–2121. https://doi.org/10.1016/0016-7037(96)00091-9

Burnham CW, Ohmoto H (1980) Late-stage processes of felsic magmatism. Min Geol Spec Issue 8:1–11

Clark AH, Arancibia ON (1995) The occurrence, paragenesis and implications of magnetite-rich alteration-mineralization in calc-alkaline porphyry copper deposits. In: Clark AH (ed) Giant ore deposits, II: Controls on the scale of orogenic magmatic-hydrothermal mineralization, Proceedings of the Second Giant Ore Deposits Workshop, April 25–27, 1995. Queens University, Kingston, pp 511–581

Einaudi MT, Hedenquist JW, Inan EE (2003) Sulfidation state of fluids in active and extinct hydrothermal systems: transitions from porphyry to epithermal environments. In: Simmons SF, Graham I (eds) Volcanic, geothermal and ore-forming fluids: rulers and witnesses of processes within the earth. Soc Econ Geol Spec Pub 10:285–313

Faure G (1986) Principles of isotope geology, 2nd edn. John Wiley, New York 589 p

Ghorbani M (2013) The economic geology of Iran: mineral deposits and natural resources. Springer, Dordrecht, 581 p. https://doi.org/10.1007/978-94-007-5625-0

Ghorbani MR, Bezenjani RN (2011) Slab partial melts from the metasomatizing agent to adakite, Tafresh Eocene volcanic rocks, Iran. Island Arc 20(2):188–202. https://doi.org/10.1111/j.1440-1738.2010.00757.x

Hemley JJ, Hunt JP (1992) Hydrothermal ore-forming processes in the light of studies in rock-buffered systems: II. Some general geologic applications. Econ Geol 87(1):23–43. https://doi.org/10.2113/gsecongeo.87.1.23

Henley RW, Truesdell AH, Barton PB, Whitney JA (1984) Fluid-mineral equilibria in hydrothermal systems. Rev Econ Geol 1:267

Holland HD, Malinin SD (1979) The solubility and occurrence of none-ore minerals. In: Barnes HL (ed) Geochemistry of hydrothermal ore deposits, 2nd edn. Wiley Interscience, New York, pp 461–508

Jahangiri A (2007) Post-collisional Miocene adakitic volcanism in NW Iran: geochemical and geodynamic implications. J Asian Earth Sci 30(3-4):433–447. https://doi.org/10.1016/j.jseaes.2006.11.008

Javidi Moghadam M, Heidarian Shahri MR, Karimpour MH (2010) Geology, mineralization, geochemistry and megnetometric studies on iron mineralization in Kalateh Shahin region, Khorasan Razavi province. J Econ Geol 1:77–96 (in Persian with an English abstract)

John DA, Garside LJ, Wallache AR (1999) Magmatic and tectonic setting of late Cenozoic epithermal gold-silver deposits in northern Nevada, with an emphasis on the Pah Rah and Virginia ranges and the northern Nevada rift. Geol Soc Nevada Spec Pub 29:65–158

Landtwing MR, Pettke T, Halter WE, Heinrich CA, Redmond PR, Einaudi MT, Kunze K (2005) Copper deposition during quartz dissolution by cooling magmatic-hydrothermal fluids: the Bingham porphyry. Earth Planet Sc Lett 235(1-2):229–243. https://doi.org/10.1016/j.epsl.2005.02.046

Maynard JB (1983) Geochemistry of sedimentary ore deposits. Springer-Verlag, 305 p. https://doi.org/10.1007/978-1-4613-9493-8

Mehrpartou M, Amini Fazl A, Radfar J (1992) Geologic map of Varzeghan. Geological Survey of Iran, scale 1:100 000, 1 sheet

Mehrpartou M, Nazeri NK (1999) Geologic map of Kaleybar. Geological Survey of Iran, scale 1:100 000, 1 sheet

Meinert LD (1995) Magmas, fluids and ore deposits. Mineral Assoc Can, Short Course Ser 23:401–418

Mollaei H, Yaghubpur AM, Sharifiyan Attar R (2009) Geology and geochemistry of skarn deposits in the northern part of Ahar batholith, East Azarbaijan, NW Iran. Iran J Earth Sci 1:15–34 (in Persian with an English abstract)

Mollai H, Sharma R, Pe-Piper G (2009) Copper mineralization around the Ahar batholith, north of Ahar (NW Iran): evidence for fluid evolution and the origin of the skarn ore deposit. Ore Geol Rev 35(3-4):401–414. https://doi.org/10.1016/j.oregeorev.2009.02.005

Nabavy H (1976) An introduction to the geology of Iran. Geological Survey of Iran, Tehran, p 109 (in Persian)

Najafzadeh Tehrani P, Calagari AA, Abedini A, Mazlumi AR (2013) The geological, mineralogical, alteration features, and rare earth elements (REEs) geochemistry of Neyzar iron deposit, southwest of Mashhad, northeast of Iran. Iran J Crystall Mineral 21:229–242 (in Persian with an English abstract)

Nicholson K (1992) Constraining mineralogical-geochemical signatures of manganese oxides: Gudies to metallogenesis. Econ Geol 87(5):1253–1264. https://doi.org/10.2113/gsecongeo.87.5.1253

Ohmoto H (1972) Systematics of sulfur and carbon isotopes in hydrothermal ore deposits. Econ Geol 67(5):551–579. https://doi.org/10.2113/gsecongeo.67.5.551

Ohmoto H, Rye RO (1979) Isotopes of sulfur and carbon. In: Barnes HL (ed) Geochemistry of Hydrothermal Ore Deposits, 2nd edn. John Wiley and Sons, New York, pp 509–567

Paterson JT, Cloos M (2005) Grasberg porphyry Cu-Au deposit, Papua, Indonesia: 2. Pervasive hydrothermal alteration. In: Porter TM (ed) Super Porphyry Copper and Gold Deposits. A global Perspective, vol 2. PGC Publishing, Adelaide, pp 331–355

Rajabzadeh MA, Rasti S (2011) Mineralization study on Dehbid magnetite deposit, Fars, using mineralogical and geochemical data. J Econ Geol 2:217–230 (article in Persian with an abstract in English)

Toth JR (1980) Deposition of submarine crusts rich in manganese and iron. Geol Soc Am Bull 91(1):44–54. https://doi.org/10.1130/0016-7606(1980)91<44:DOSCRI>2.0.CO;2

Ulrich T, Heinrich CA (2002) Geology and alteration geochemistry of the porphyry Cu-Au deposit at Bajo de la Alumbrera, Argentina. Econ Geol 97(8):1865–1888. https://doi.org/10.2113/gsecongeo.97.8.1865

Whitney DL, Evans BW (2010) Abbreviations for names of rock-forming minerals. Am Mineral 95(1):185–187. https://doi.org/10.2138/am.2010.3371

Wood SA (1998) Calculation of activity-activity and log fO_2-pH diagrams. In: Richards JP, Larson PB (eds) Techniques in hydrothermal ore deposits geology, Rev Econ Geol, vol 10, pp 81–96

Zarabi Rad R (2008) Geology, mineralogy and genesis of Ileh iron prospect, southwest of Taibad (east Iran). MSc thesis, University of Tabriz, Tabriz, Iran, 81 p